Correlated transport in silicene-based Josephson junctions

Hai Li,[1] Rui Wang,[1,2] and C. S. Ting[1]

[1]*Department of Physics and Texas Center for Superconductivity, University of Houston, Houston, Texas 77204, USA*

[2]*National Laboratory of Solid State Microstructures and Department of Physics, Nanjing University, Nanjing 210093, China*

(Received 18 May 2016; revised manuscript received 5 August 2016; published 24 August 2016)

We theoretically investigate the effects of exchange splitting, electric field and strain on the supercurrent in silicene-based Josephson junctions. It is observed that a $0-\pi$ transition is induced by the exchange splitting, and the critical supercurrent at the transition point is nonvanishing. Owing to the unique buckling structure of silicene, the supercurrent can be effectively controlled by the electric field. For the strain dressed supercurrent, it is revealed that the current-phase relation is profoundly influenced by the strain, and the supercurrent exhibits a switch effect with increasing the strength of strain. These findings will potentially provide some intriguing insights into the correlated transport in silicene-based Josephson junctions.

DOI: 10.1103/PhysRevB.94.085422

I. INTRODUCTION

As a graphenelike allotrope of silicon [1–5], silicene has been successfully synthesized on a variety of substrates such as Ag (111) [6–8], $ZrB_2(0001)$ [9], Ir (111) [10], and MoS_2 [11]. It is demonstrated that silicene possesses a nonvanishing spin-orbit coupling (SOC) induced energy gap at the Dirac point [12], offering an opportunity for the detection of quantum spin Hall states [13–15]. Remarkably, since a stable silicene sheet prefers a low buckling structure [16], the energy gap can be effectively tuned by an electric field perpendicular to the sheet plane [17,18]. These fascinating properties together with the compatibility with silicon-based electronics make silicene a promising candidate for logic applications [19]. Recently, several proposals have been put forward to tailor the electronic properties of silicene including the superconductivity [20–22]. Based on first-principle calculations, some theoretical work reported that a doped silicene performs superconductivity under an external electric field [20] or a biaxial tensile strain [21]. Most importantly, in terms of the scanning tunneling spectroscopy, Chen *et al.* observed that an Ag (111) supported silicene exhibits superconductivity [22]. These significant achievements offer a solid foundation for exploring the superconducting correlations in silicene-based Josephson junctions [23].

Superconducting (S) correlations can penetrate through the nonsuperconducting (N) region of a Josephson junction [24,25] via multiple Andreev reflections (ARs) [26–28]. In the N region, the quantum interferences between incident quasiparticles and Andreev excitations generate a series of discrete Andreev bound states (ABSs), which are responsible for the supercurrent especially in the short-junction limit $d \ll \xi_0$ (with d the junction length and ξ_0 the superconducting coherence length) [29]. For a dc Josephson junction in thermal equilibrium, a nonvanishing phase difference (ϕ) between the two superconducting electrodes is required to generate a finite supercurrent [25]. The connection between supercurrent and ϕ is described by the current-phase relation (C Φ R), which is essential for understanding the fundamental properties of Josephson junctions. In general, the simplest C Φ R can be approximately parameterized by a standard sinusoidal function, coinciding with the so-called 0 junction which possesses a ground state at $\phi = 0$. However, if the N region is occupied by a magnetoactive material such as the ferromagnetic (F) metal, the ground state undergoes a phase shift of π and the corresponding supercurrent reverses the direction, leading to a π junction. Moreover, a $0-\pi$ transition may occur in a S/F/S junction [30–35], due to the phase jumps at the S/F interfaces as well as the oscillations of order parameters within the F region. Intriguingly, in graphene-based S/F/S junctions, the critical supercurrent at the transition point is finite, which is favorable for the application of dissipationless supercurrent switch [36,37].

Motivated by the remarkable electronic structures of silicene [12,16–18] as well as the significant achievements in the fabrication of silicene-based nanodevices [6–11,19], in this paper we propose a silicene-based S/F/S junction and investigate the influences of electric field and exchange splitting on the ABS and supercurrent. It is observed that a $0-\pi$ transition is induced by the exchange splitting, and the critical supercurrent at the transition point is nonvanishing. Remarkably, the supercurrent can be effectively controlled by the electric field. This exotic property results from the unique buckling structure of silicene, which is absent in graphene-based Josephson junctions [36,37]. Additionally, it is found that the configuration of the supercurrent is dependent on the temperature.

Moreover, it is worth noting that the supporting substrate may inevitably induce strain in the silicene sheet [15,38–41], resulting in the shift of Dirac point as well as the distortion of Dirac cone. With this in mind, we also consider the strain dressed supercurrent in a silicene-based S/strained/S junction. It is revealed that the configuration of CΦR strongly depends on the shift of Dirac point, and the supercurrent is electrically tunable. More importantly, the supercurrent exhibits a switch effect with increasing the displacement of Dirac point. These findings are favorable for the applications in silicene-based Josephson junctions.

The organization of this paper is as follows. In Sec. II, we discuss the ABS as well as the electrically controllable supercurrent in a silicene-based S/F/S junction. Then, in Sec. III we consider the strain dressed supercurrent in a silicene-based S/strained/S junction and demonstrate a switch effect can be realized in this setup. Finally, the conclusion and a brief summary appear in Sec. IV.

II. EXCHANGE SPLITTING AND ELECTRIC FIELD MODULATED SUPERCURRENT

In this section, we present a silicene-based S/F/S junction and investigate the influences of exchange splitting and electric field on the supercurrent. Since the density of state becomes independent on ϕ for $\varepsilon \gg \Delta_0$ [29], we restrict ourselves to the energy regime of $|\varepsilon| \lesssim \Delta_0$.

A. Model and method

The proposed setup is schematically shown in Fig. 1, where a silicene sheet is placed in the xy plane, with a ferromagnetic layer covering the middle region ($0 < x < d$) and two superconducting electrodes coating regions $x < 0$ and $x > d$, respectively. To tune the energy gap, we apply an electric field (E_z) along the z direction. In the frame of the Dirac-Bogoliubov-de Gennes (DBdG) equation, the ABS and dc supercurrent along the x direction is calculated by employing the scattering approach. The DBdG Hamiltonian, in the basis of $\psi_k^\dagger = \{(\psi_{k\sigma}^A)^\dagger, (\psi_{k\sigma}^B)^\dagger, \psi_{-k\bar{\sigma}}^A, \psi_{-k\bar{\sigma}}^B\}$, is given by [23,42]

$$\mathcal{H} = \begin{pmatrix} H_0 - \sigma h(x) & \sigma\Delta(x) \\ \sigma\Delta^\dagger(x) & -(H_0 - \bar{\sigma}h(x)) \end{pmatrix}, \tag{1}$$

where $H_0 = \hbar v_F(\eta k_x\tau_x - k_y\tau_y) + m_{\eta\sigma}\tau_z - \mu\tau_0$ is the effective Hamiltonian describing the low-lying physics of silicene [12]. $k = (k_x, k_y)$ is the two-dimensional momentum measured with respect to Dirac points, $\hat{\tau} = (\tau_x, \tau_y, \tau_z)$ is the Pauli matrix operating on the sublattice space, and τ_0 is a 2×2 unit matrix; $\eta = \pm 1$ labels the K (K′) valley, $\sigma = \pm 1$ is the spin index with $\bar{\sigma} = -\sigma$, μ is the Fermi energy, and v_F indicates the Fermi velocity. The effective mass term $m_{\eta\sigma} = lE_z - \eta\sigma\lambda_{\rm SO}$, with $\lambda_{\rm SO}$ the strength of SOC; lE_z results from the buckling structure together with an external electric field E_z, with $2l$ indicating the separation between the A and B sublattices in the z direction.

The superconductivity in S regions can be proximity induced by superconducting electrodes, and this approach has been successfully employed in graphene-based devices [43–49]. To ensure the validity of the mean-field approximation, the Fermi energy $\mu_{\rm S}$ in the S region should be much larger than the superconducting gap Δ_0, viz. $\mu_{\rm S} \gg \Delta_0$ should be satisfied [42]. Furthermore, we assume that the Fermi wavelength $\lambda_{\rm F}$ in the F region is large enough compared to $\lambda_{\rm S}$, so that the pair potential can be rationally described by a step function [50–52],

$$\Delta(x) = \Delta_0[e^{i\phi_{\rm L}}\Theta(-x) + e^{i\phi_{\rm R}}\Theta(x-d)], \tag{2}$$

where $\Theta(x)$ labels the Heaviside step function, and the phase difference can be defined as $\phi = \phi_{\rm R} - \phi_{\rm L}$. In the F region, the exchange splitting can be achieved by depositing a ferromagnetic insulator on the top of a silicene sheet [53], as that has been realized recently in a graphene/yttrium iron garnet structure [54]. Taking an abrupt approximation [50–52], the exchange field in the F region can be written as

$$h(x) = h_0\Theta(x)\Theta(d-x), \tag{3}$$

with h_0 being the strength of exchange splitting.

To calculate the ABS and supercurrent, we first construct the scattering states which can be derived from the DBdG equation $\mathcal{H}\psi_k = \varepsilon\psi_k$. Accordingly, the wave function in the left (right) S region is a linear combination of an electronlike state $\psi_{\rm S}^{e-(+)}$ and a holelike state $\psi_{\rm S}^{h-(+)}$ with amplitudes $a_{\rm L(R)}$ and $b_{\rm L(R)}$, respectively, and which can be formulated as,

$$\Psi_{\rm L(R)}^{\rm S} = a_{\rm L(R)}\psi_{\rm S}^{e-(+)} + b_{\rm L(R)}\psi_{\rm S}^{h-(+)}, \tag{4}$$

where $\pm$ indicate the propagation directions (along $\pm\hat{x}$) that should be determined by the corresponding group velocities [55]. The detailed structures of $\psi_{\rm S}^{e(h)\pm}$, after omitting the trivial factor $e^{ik_y y}$, can be written as,

$$\psi_{\rm S}^{e+(-)} = e^{[+(-)ik_0x-(+)\kappa x]}\begin{pmatrix} +(-)\eta\sigma e^{i[+(-)\eta\vartheta_{\rm S}+\beta]} \\ \sigma e^{i\beta} \\ +(-)\eta e^{i[+(-)\eta\vartheta_{\rm S}-\phi_{\rm R(L)}]} \\ e^{-i\phi_{\rm R(L)}} \end{pmatrix}, \tag{5a}$$

$$\psi_{\rm S}^{h+(-)} = e^{[-(+)ik_0x-(+)\kappa x]}\begin{pmatrix} -(+)\eta\sigma e^{i[-(+)\eta\vartheta_{\rm S}-\beta]} \\ \sigma e^{-i\beta} \\ -(+)\eta e^{i[-(+)\eta\vartheta_{\rm S}-\phi_{\rm R(L)}]} \\ e^{-i\phi_{\rm R(L)}} \end{pmatrix}, \tag{5b}$$

where $\vartheta_{\rm S} = \sin^{-1}(k_y/\mu_{\rm S})$ and $\beta = \cos^{-1}(\varepsilon/\Delta_0)\Theta(\Delta_0 - \varepsilon) - i\cosh^{-1}(\varepsilon/\Delta_0)\Theta(\varepsilon - \Delta_0)$. In the limit of $\mu_{\rm S} \gg \mu$ (μ is the chemical potential in the region of $0 < x < d$), $k_0 = \mu_{\rm S}$ and $\kappa = \sqrt{\Delta_0^2 - \varepsilon^2}$. For the brevity of notation, we set $\hbar v_F \equiv 1$ throughout this work.

As regards the F region, in the absence of spin-flip scattering, an incoming electron (hole) with fixed energy ε and spin σ, is either Andreev-reflected as an isoenergetic hole (electron) stemming from the spin $\bar{\sigma}$ hole (electron) band, or normally reflected as an electron (a hole) of the same energy and spin. As a consequence, the wave function inside the F region can be expressed as

$$\Psi^{\rm F} = \sum_{p=e,h}\sum_{q=\pm} c^{pq}\psi_{\rm F}^{pq}, \tag{6}$$

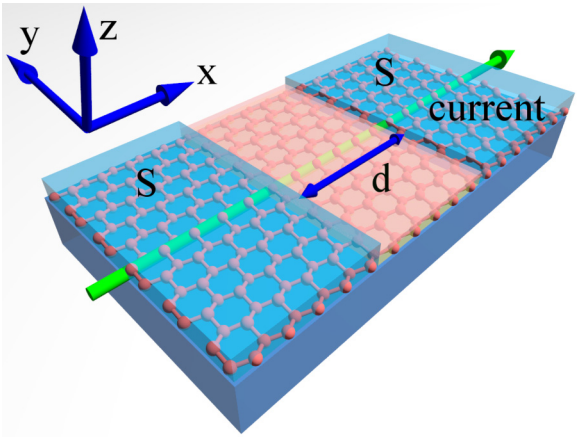

FIG. 1. Schematic of a silicene-based Josephson junction.

where the related scattering coefficients are denoted by c^{pq}, and the basis scattering states $\psi_{\rm F}^{pq}$ are explicitly given by

$$\psi_{\rm F}^{e\pm}=\frac{e^{\pm ik_x^e x}}{\sqrt{2e^{s_+\gamma_+}\cos\alpha_+}}\begin{pmatrix}\pm\eta e^{\pm i\eta s_+\alpha_+}\\ e^{-s_+\gamma_+}\\ 0\\ 0\end{pmatrix}, \tag{7a}$$

$$\psi_{\rm F}^{h\pm}=\frac{e^{\pm ik_x^h x}}{\sqrt{2e^{-s_-\gamma_-}\cos\alpha_-}}\begin{pmatrix}0\\ 0\\ \mp\eta e^{\pm i\eta s_-\alpha_-}\\ e^{s_-\gamma_-}\end{pmatrix}, \tag{7b}$$

where the factors $1/\sqrt{2e^{s_+\gamma_+}\cos\alpha_+}$ and $1/\sqrt{2e^{-s_-\gamma_-}\cos\alpha_-}$ ensure that all states carry the same amount of quasiparticle current. The trivial factor $e^{ik_y y}$ is omitted for simplicity of notation, and the corresponding parameters are defined as $s_{+(-)}=\mathrm{sgn}\,(\varepsilon+\sigma h_0+(-)\mu)$, $k^{e(h)}=\sqrt{(\varepsilon+\sigma h_0+(-)\mu)^2-m_{\eta\sigma}^2}$, $\alpha_{+(-)}=\sin^{-1}(k_y/k^{e(h)})$, $k_x^{e(h)}=s_{+(-)}k^{e(h)}\cos\alpha_{+(-)}$, and $\gamma_{+(-)}=\sinh^{-1}(m_{\eta\sigma}/k^{e(h)})$. The signs of $k_x^{e(h)}$ are determined to ensure the group velocities of the incidence (reflection) states are positive (negative).

In our calculation, the width (W, along the y direction) of the junction is assumed to be much larger than the junction length, i.e., $W\gg d$, so that the edge effects can be rationally neglected and the translational invariance in the y direction is preserved. Consequently, resorting to the conversation of the transverse momentum k_y, the relation between the AR angle α_- and incident angle α_+ can be parameterized as

$$\frac{\sin\alpha_-}{\sin\alpha_+}=\frac{\mathrm{sgn}\,(\varepsilon+\sigma h_0+\mu)\sqrt{(\varepsilon+\sigma h_0+\mu)^2-m_{\eta\sigma}^2}}{\mathrm{sgn}\,(\varepsilon+\sigma h_0-\mu)\sqrt{(\varepsilon+\sigma h_0-\mu)^2-m_{\eta\sigma}^2}}, \tag{8}$$

which uncloses the configurations of AR under the influences of exchange splitting and electric field. Especially, in the case of $|\varepsilon+\sigma h_0\pm\mu|>|m_{\eta\sigma}|$, Eq. (8) predicts a specular AR where an incident electron in the conduction (valence) band is specularly reflected as a hole stemming from the valence (conduction) band. The specular AR is a unique scenario which arises in superconducting junctions based on Dirac fermion materials such as graphene [42] and silicene [23].

Taking care of the current conservation in the x direction, the boundary conditions can be obtained by matching the relevant wave functions at boundaries $x=0$ and $x=d$, as shown in Appendix. After some mathematical handing, the boundary conditions can also be described into the relations between hole and electron wave functions,

$$\psi^h|_{x=d(0)}=\Omega_{+(-)}\psi^e|_{x=d(0)}, \tag{9}$$

and the connections between electron (hole) wave functions located at the two boundaries,

$$\psi^{e(h)}|_{x=d}=\Lambda_{+(-)}\psi^{e(h)}|_{x=0}, \tag{10}$$

where Eq. (6) has been rewritten as $\Psi_{\rm F}\equiv(\psi^e,\psi^h)^T$. The corresponding transfer matrices are give by

$$\Omega_\pm=\frac{\sigma e^{-i\phi^{R(L)}}}{\cos\vartheta_S}\begin{pmatrix}\cos(\beta\mp\eta\vartheta_S) & \mp i\eta\sin\beta\\ \mp i\eta\sin\beta & \cos(\beta\pm\eta\vartheta_S)\end{pmatrix}, \tag{11}$$

and

$$\Lambda_\pm=\frac{1}{\cos\alpha_\pm}\begin{pmatrix}\cos(\theta_\pm+\eta s_\pm\alpha_\pm) & \pm i\eta e^{\pm s_\pm\gamma_\pm}\sin\theta_\pm\\ \pm i\eta e^{\mp s_\pm\gamma_\pm}\sin\theta_\pm & \cos(\theta_\pm-\eta s_\pm\alpha_\pm)\end{pmatrix}, \tag{12}$$

where $\theta_{+(-)}=k_x^{e(h)}d$. According to the approach proposed in Ref. [56], the ABSs can be determined by the condition

$$\mathrm{Det}(\tau_0-\Lambda_+^{-1}\Omega_+^{-1}\Lambda_-\Omega_-)=0. \tag{13}$$

After some lengthy algebra, we arrive at

$$\mathcal{A}\cos 2\beta+\mathcal{B}\sin 2\beta=\mathcal{C}, \tag{14}$$

which contains the bound energy $\varepsilon_{\eta\sigma}$ via the relation $\beta=\cos^{-1}(\varepsilon_{\eta\sigma}/\Delta_0)\Theta(\Delta_0-\varepsilon_{\eta\sigma})-i\cosh^{-1}(\varepsilon_{\eta\sigma}/\Delta_0)\Theta(\varepsilon_{\eta\sigma}-\Delta_0)$, and the general expressions of coefficients $\mathcal{A}$, $\mathcal{B}$, and $\mathcal{C}$ are explicitly given in Appendix.

In the present work, we concentrate on the stationary Josephson effect within the regime of $d\ll\xi_0$ ($\xi_0\sim 1/\Delta_0$). The supercurrent, carried by the discrete ABSs, can be formulated as [23,36,37,53,56–64]

$$\mathcal{I}(\phi)=-\frac{e}{\hbar}\sum_{\eta\sigma}\int_{-\frac{\pi}{2}}^{\frac{\pi}{2}}d\alpha_+\cos\alpha_+\sum_{n=0}^{N_{\eta\sigma}}\tanh\left(\frac{\varepsilon_{\eta\sigma}^n}{2k_{\rm B}T}\right)\frac{{\rm d}\varepsilon_{\eta\sigma}^n}{{\rm d}\phi}, \tag{15}$$

where $k_{\rm B}$ denotes the Boltzmann constant, T labels the temperature, and $N_{\eta\sigma}=\frac{W}{2\pi}\sqrt{(\varepsilon_{\eta\sigma}+\mu+\sigma h_0)^2-m_{\eta\sigma}^2}$ indicates the number of transverse modes. It should be noted that the bound energy $\varepsilon_{\eta\sigma}^n$ takes positive values. For the sake of convenience, we introduce a quantity $I_0=\frac{e\Delta_0}{2\hbar}\sum_{\eta\sigma}N_{\eta\sigma}$, so that the normalized supercurrent can be defined as $I(\phi)=\mathcal{I}(\phi)/I_0$. In addition, the experimentally measurable critical supercurrent can be defined as

$$I_c=|\max\,[I(\phi)]|. \tag{16}$$

Accordingly, the $0-\pi$ transition manifests itself as a cusp in the I_c curves.

B. Josephson effect in a S/F/S junction with an undoped F region ($\mu=0$)

In this subsection, we propose a S/F/S junction with a undoped F region ($\mu=0$) and discuss the influences of the exchange splitting and electric field on the ABS and supercurrent.

1. *Configuration of the ABS*

In the case of $\mu=0$, a simple inspection of Eq. (8) leads to the relation $\alpha_-=\alpha_+\equiv\alpha$, indicating a perfectly specular AR occurring at the two FS interfaces. Without loss of generality, we choose $h_0=\mu_S$ to obtain analytical results. In doing so, the valley- and spin-resolved ABSs $\pm\varepsilon_{\eta\sigma}$ ($\varepsilon_{\eta\sigma}\geqslant 0$) can be

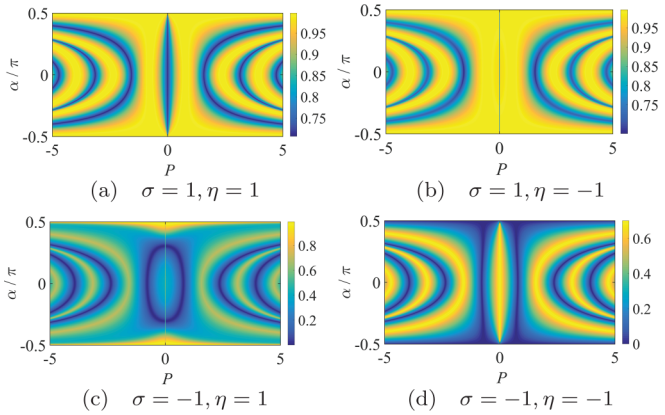

FIG. 2. Contour plots of spin- and valley-resolved Andreev bound states, where $lE_z = \lambda_{SO} = 5\Delta_0$, $d/\xi_0 = 0.05$, and $\phi = \pi/2$. For $\eta\sigma = 1$, $m_{\eta\sigma} = 0$, panels (a) and (d) are consistent with the results reported in Ref. [36].

analytically formulated as

$$\varepsilon_{\eta\sigma} = \frac{\Delta_0}{\sqrt{2\mathcal{M}}} \times \sqrt{\mathcal{M}+\mathcal{N}+\sigma \sin(2P\cos\alpha)\cosh\gamma\cos^2\alpha\sqrt{\mathcal{M}-\mathcal{D}}}, \tag{17}$$

with related parameters being defined as

$$\mathcal{M} = \cos^4\alpha[\cos^4\alpha + 4\sin^2\alpha\sin^2(P\cos\alpha)] + [\sin^4(P\cos\alpha)\sinh^2\gamma + 2\cos^4\alpha\sin^2(P\cos\alpha) \times \cos(2P\cos\alpha) + 4\cos^2\alpha\sin^4(P\cos\alpha)]\sinh^2\gamma, \tag{18a}$$

$$\mathcal{N} = \cos^6\alpha[\cos^2\alpha - 2\sin^2(P\cos\alpha)]\cos\phi + \sinh^2\gamma \times \{\cos 2\alpha\cos^2\alpha\sin^2(P\cos\alpha)[\cos^2\alpha - 2\sin^2(P\cos\alpha)] - \sin^2(P\cos\alpha)\cos^4\alpha\cos\phi - \sin^4(P\cos\alpha)\cos 2\alpha\sinh^2\gamma\} \tag{18b}$$

$$\mathcal{D} = [\cos^4\alpha\cos\phi + \sin^2(P\cos\alpha)\cos 2\alpha\sinh^2\gamma]^2, \tag{18c}$$

where $\alpha = \sin^{-1}(k_y/\sqrt{h_0^2 - m_{\eta\sigma}^2})$, $P = d\sqrt{h_0^2 - m_{\eta\sigma}^2}$, and $\gamma = \sinh^{-1}(m_{\eta\sigma}d/P)$. The parameter P is spin- and valley-dependent, which depicts the effects of the exchange splitting strength h_0, the effective mass $m_{\eta\sigma}$, and the junction length d. In the case of $m_{\eta\sigma} = 0$, one can readily verify that Eq. (17) reproduces the results in Ref. [36], as shown in the panels (a) and (d) of Fig. 2.

To figure out the textures of ABSs under the influence of exchange splitting, we present the contour plots of ABSs with the phase difference being fixed to $\phi = \pi/2$, as shown in Fig. 2. Since the exchange splitting breaks the so called spin $\otimes$ valley symmetry [23], the ABSs are spin- and valley-resolved. This point is quite different from that in similar graphene-based models where the ABSs are valley degeneracy [36]. It is observed that the ABSs periodically oscillate with respect to the parameter P, but the corresponding oscillatory amplitudes never decay with increasing P. The striking oscillatory texture without a damping envelope can be attributed to the Dirac characteristic of the excitations in silicene. Because the exchange splitting induced momentum mismatch $[2h_0/(\hbar v_F)]$ between the Andreev correlated electron and hole is proportional to the exchange splitting strength, the oscillations become more pronounced with increasing P (or equivalently, h_0 for fixed d and $m_{\eta\sigma}$). Additionally, in the limit of $P = 0$, i.e., $|h_0| = |m_{\eta\sigma}|$, Eq. (17) can be simplified as $\varepsilon_{\eta\sigma} = \Delta_0\cos(\phi/2)$, which is independent of the spin and valley indices.

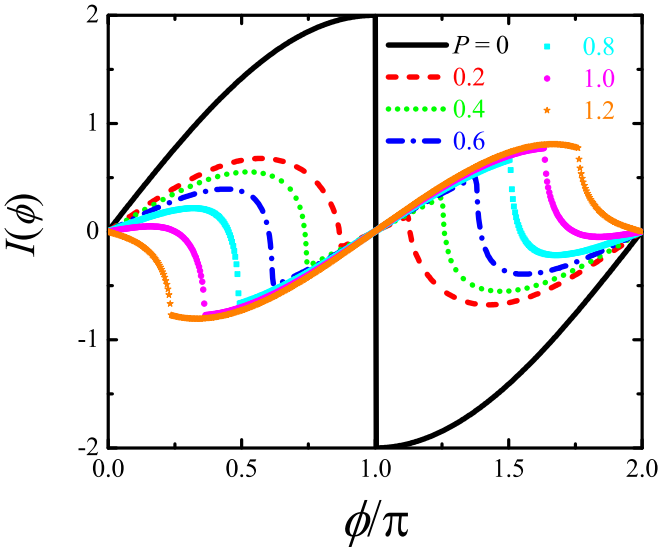

FIG. 3. C Φ R in a silicene-based S/F/S junction with $\mu = 0$, where $lE_z/\lambda_{SO} = 2$ and $d/\xi_0 = 0.05$.

2. *Electrically controllable supercurrent*

Accordingly, the CΦR can be obtained by substituting Eq. (17) into Eq. (15), and the resulting CΦR for various values of P at zero temperature are shown in Fig. 3. A prominent character of the CΦR is the appearance of the $0-\pi$ transition with increasing the parameter P, and this scenario originates from phase jumps at the S/F interfaces. We note that the amplitude of CΦR only oscillates with increasing P but never decays with respect to it, this characteristic is quite different from that in ordinary Josephson junctions [25]. It is also found that the envelope of the CΦR deviates from the conventional sinusoidal form, indicating the existence of higher harmonics components. In passing, as proposed in Ref. [36], the discontinuity of CΦR at $\phi = \pi$ for $P = 0$ can be ascribed to the crossing of ABSs.

The P-dependent critical supercurrents at zero temperature are illustrated in Fig. 4. As seen, the $I_c - P$ curves host legible cusps and undamped oscillations. According to the definition given by Eq. (16), the proposed cusp is the manifestation of the $0-\pi$ transition. A further inspection of the cusps reveals that the critical supercurrent at the transition point never approaches to zero; this significant characteristic is quite different from that in ordinary Josephson junctions where the excitations are described by the Schrödinger equation [25]. In the present system, the undamped oscillations and

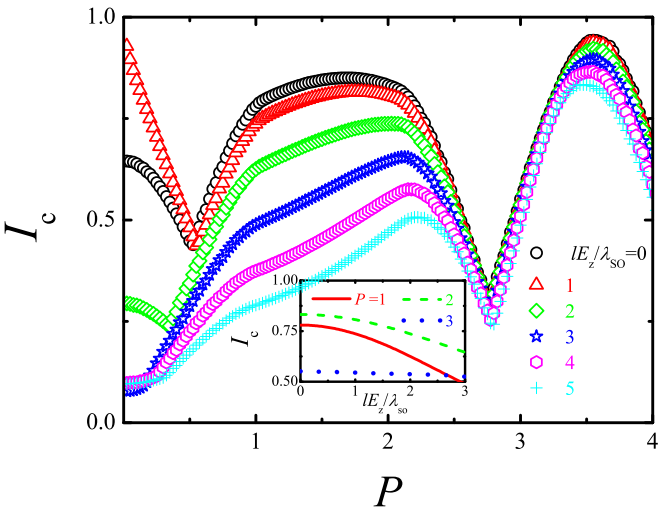

FIG. 4. Critical supercurrent in a silicene-based S/F/S junction with $\mu = 0$ and $d/\xi_0 = 0.1$, where the inset exhibits the dependence of critical supercurrent on the electric field.

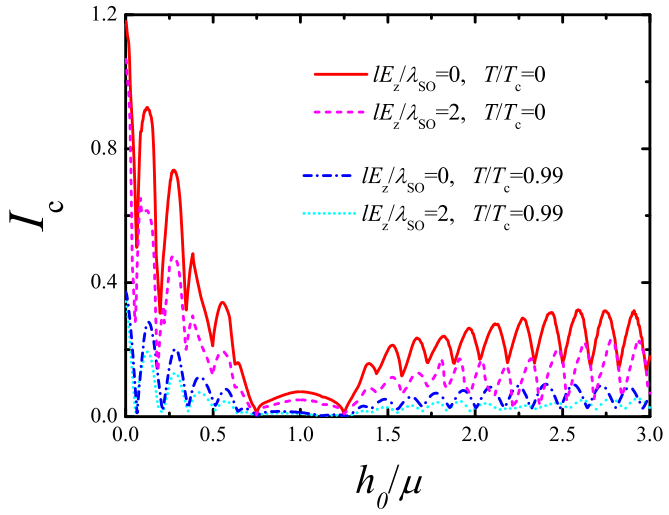

FIG. 5. Critical supercurrent as a function of the exchange splitting strength in a silicene-based S/F/S junction with $\mu d = 10$.

nonvanishing critical supercurrent at the transition point can be attributed to the Dirac-like low-energy excitations of silicene.

Owing to the buckling structure, the band character of silicene can be effectively tuned by a perpendicular electric field (lE_z). This unique property is also manifested in the electric field dressed $I_c - P$ curves. For a small P (e.g., $0 < P \lesssim 2.3$), by comparing the $I_c - P$ curves corresponding to different values of lE_z, one can find that the critical supercurrent can be effectively controlled by a perpendicular electric field (see Fig. 4). This remarkable scenario can be regarded as the most prominent feature in a silicene-based S/F/S junction, and which cannot be realized in graphene-based S/F/S junctions [36,37]. To further elucidate the influences of the electric field on the critical supercurrent, we calculate the critical supercurrent as a function of lE_z, as illustrated in the inset of Fig. 4. It is observed that the electrical tunability of critical supercurrent disappears almost completely in the P-dominated regime (e.g., $P \gtrsim 2.3$), which implies that there exists a competition between the electric field and exchange splitting on the modulation of the critical supercurrent. Since the energy gap ($E_{\rm gap} = 2|lE_z - \eta\sigma\lambda_{\rm SO}|$) is proportional to the electric field in the regime of $lEz \geqslant \lambda_{\rm SO}$, the critical supercurrent decreases with increasing the electric field when $lEz \geqslant \lambda_{\rm SO}$.

In addition, we note that recently D. Kuzmanovski *et al.* reported that the $0 - \pi$ transition is electrically controllable in a silicene-based F/S/F junction [64]. This intriguing phenomenon is also found in Fig. 4. By inspecting the $I_c - P$ curves in the regime of $P < 1$, one can find that the $0 - \pi$ transition arises only for a small electric field (e.g., $lE_z/\lambda_{\rm SO} = 0,1,2$) and completely disappears when the electric field is large enough (e.g., $lE_z/\lambda_{\rm SO} = 3,4,5$). In this regard, the $0 - \pi$ transition can be controlled by an electric field.

C. Supercurrent in a S/F/S Junction with a doped F region ($\mu \neq 0$)

We now turn to the supercurrent in the S/F/S junction with a finite μ. For the sake of simplicity we only consider the limit of $\mu_{\rm S} \gg \mu_{\rm F}$, so that $\vartheta_{\rm S} \simeq 0$. Consequently, after a straightforward calculation, Eq. (14) can be reduced to

$$\begin{aligned}\cos\phi = &\left(\frac{\cos\theta_+\sin\theta_-\cosh\gamma_-}{\cos\alpha_-} + \frac{\cos\theta_-\sin\theta_+\cosh\gamma_+}{\cos\alpha_+}\right)\\ &\times \sin 2\beta\\ &+\left(\cos\theta_+\cos\theta_- - \frac{\sin\theta_+\sin\theta_-}{\cos\alpha_+\cos\alpha_-}\cosh\gamma_+\cosh\gamma_-\right)\\ &\times \cos 2\beta\\ &- s_+s_-\left(\tan\alpha_+\tan\alpha_- + \frac{\sinh\gamma_+\sinh\gamma_-}{\cos\alpha_+\cos\alpha_-}\right)\\ &\times \sin\theta_+\sin\theta_-. \end{aligned} \tag{19}$$

For a strongly doped F region ($\mu \gg \Delta_0$), one can reproduce the results given in Ref. [23] by substituting $h_0 = 0$ into Eq. (19).

Combing Eqs. (15), (16), and (19), one can numerically calculate the critical supercurrent shown in Fig. 5. As can be seen, the critical supercurrent periodically oscillates with the exchange splitting strength h_0, where the sharp cusps indicate the exchange splitting induced $0 - \pi$ transitions. As indicated by Eq. (8), the configuration of the AR can be modulated by the ratio h_0/μ, thus the supercurrent should be profoundly modulated by the exchange splitting as well as the doping density and/or gate voltage in the F region. In the case of $\mu \gg \Delta_0$, the AR is of retro type for $h_0/\mu < 1$, and the amplitude of I_c decreases with h_0/μ. In contrast, the oscillatory curve hosts an increasing envelop in the range of $h_0/\mu > 1$ where the AR becomes specular. Significantly, due to the electrically tunable band gap, the amplitude of I_c can also be controlled by an electric field.

We also investigate the influences of temperature (T) on the critical supercurrent, as illustrated in Fig. 5. A careful comparison between the red solid and blue dashed-dot curves (or equivalently, between the magenta dashed and cyan dot curves) reveals that the position of $0 - \pi$ transition point, i.e., $[h_0/\mu]_{\rm T}$, is dependent on the temperature. Moreover, the temperature dependence of $[h_0/\mu]_T$ behaves differently in the

two regimes of $h_0/\mu < 1$ and $h_0/\mu > 1$. For $h_0/\mu < 1$, the value of $[h_0/\mu]_{\rm T}$ increases with rising temperature, while in the case of $h_0/\mu > 1$, the enhancement of temperature leads to the decline of the value of $[h_0/\mu]_{\rm T}$. In addition, the correlated transport is suppressed with increasing temperature.

III. STRAIN DRESSED JOSEPHSON EFFECTS

In this section, we discuss the influences of local strain and electric field on the correlated transport in a silicene-based S/strained/S junction. The strain induced deformations are assumed to be elastic and smooth. In principle, the proposed strain can be achieved by the deformable substrates on which silicene sheets are deposited, as that has been proposed in graphene-based counterparts [65–67].

A. Model

The geometry of S/strained/S junction is the same as that of S/F/S junction shown in Fig. 1, except that the middle region of the present junction is occupied by a strained silicene. It is demonstrated that a strain [40], on one hand, results in the shift of Dirac points in the momentum space, with the displacements in the two valleys being opposite to each other. On the other hand, the strain also dresses the Fermi velocity anisotropically, leading to the distortions of Dirac cones. To the leading order of q, the effective low-energy Hamiltonian of strained silicene, can be formulated as [68,69]

$$H_{\rm st} = \hbar v_F(\eta\iota_x q_x\tau_x - \iota_y q_y\tau_y) + m_{\eta\sigma}\tau_z - \mu\tau_0, \qquad (20)$$

where $q = (q_x, q_y)$ is measured with respect to the shifted Dirac points, i.e., $q = k - q_D$, and the valley-dependent displacement $q_D \equiv \eta(q_{Dx}, q_{Dy})$. $\iota_{x(y)} = v_{x(y)}/v_F$ depicts the distortion of Dirac cone, with $v_{x(y)}$ being the distorted Fermi velocity along the $x(y)$ direction. It is worth noting that the applied strain may also change the chemical potential μ and the separation $(2l)$ between the sublattices A and B. Nevertheless, the deviations of μ can be offset by gating and/or doping the strained region. Since variation of l only takes action on the effective mass in the presence of external electric fields, one can compensate the deviated effective mass by rationally tuning the electric field. Therefore, the deviations of μ and l do not play essential roles in the correlated transport.

In the strained region, the corresponding DBdG equation takes the form

$$\begin{pmatrix} H_{\rm st} & 0 \\ 0 & -H_{\rm st} \end{pmatrix}\begin{pmatrix} u_{\rm st} \\ v_{\rm st} \end{pmatrix} = \varepsilon\begin{pmatrix} u^e_{\rm st} \\ v^h_{\rm st} \end{pmatrix}, \qquad (21)$$

where $(u_{\rm st}, v_{\rm st})^T \equiv \psi_{\rm st}$. Accordingly, the basis scattering states can be derived as

$$\psi^{e\pm}_{\rm st} = \frac{e^{(\pm iq^e_x x + ik_y y)}}{\sqrt{2\iota_x e^{s^{\rm st}_+\gamma^{\rm st}_+}\cos\alpha^{\rm st}_+}}\begin{pmatrix} \pm\eta e^{\pm i\eta s^{\rm st}_+\alpha^{\rm st}_+} \\ e^{-s^{\rm st}_+\gamma^{\rm st}_+} \\ 0 \\ 0 \end{pmatrix}, \qquad (22a)$$

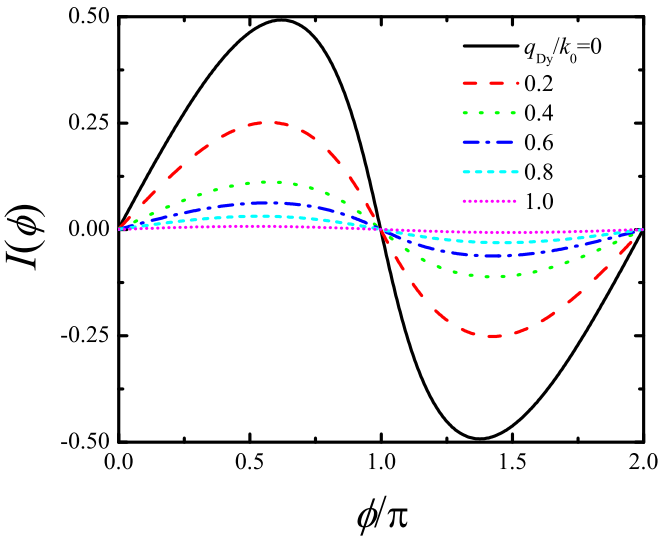

FIG. 6. C Φ R in a silicene-based S/strained/S junction. Where $\mu/\Delta_0 = 20$, $\mu_S/\Delta_0 = 100$, and the other parameters are taken the same values as that in Fig. 3.

$$\psi^{h\pm}_{\rm st} = \frac{e^{(\pm iq^h_x x + ik_y y)}}{\sqrt{2\iota_x e^{-s^{\rm st}_-\gamma^{\rm st}_-}\cos\alpha^{\rm st}_-}}\begin{pmatrix} 0 \\ 0 \\ \mp\eta e^{\pm i\eta s^{\rm st}_-\alpha^{\rm st}_-} \\ e^{s^{\rm st}_-\gamma^{\rm st}_-} \end{pmatrix}, \qquad (22b)$$

with the involved parameters being defined as: $s^{\rm st}_{+(-)} = {\rm sgn}(\varepsilon + (-)\mu)$, $q^{e(h)} = \sqrt{(\varepsilon + (-)\mu)^2 - m^2_{\eta\sigma}}$, $\alpha^{\rm st}_{+(-)} = \sin^{-1}[\iota_y(k_y - \eta q_{Dy})/q^{e(h)}]$, $q^{e(h)}_x = s^{\rm st}_{+(-)}\iota_x^{-1}q^{e(h)}\cos\alpha^{\rm st}_{+(-)}$, and $\gamma^{\rm st}_{+(-)} = \sinh^{-1}(m_{\eta\sigma}/q^{e(h)})$. Correspondingly, one can define $\theta^{\rm st}_{+(-)} = q^{e(h)}_x d$. The wave function in the strained region can be obtained by replacing $\psi^{pq}_{\rm F}$ with $\psi^{pq}_{\rm st}$ in Eq. (6), and the strain dressed ABSs and supercurrent can be achieved by employing the same procedure proposed in Sec. II A.

B. Results and discussion

Both the displacements and distortions of Dirac cones are significantly responsible for the correlated transport. We first discuss the supercurrent under the influences of the displacements of Dirac points. As the q_{Dx} hardly takes action on the transport in the x direction [68,69], we mainly consider the effect of q_{Dy} on the supercurrent. Figure 6 illustrates the strain dressed CΦR corresponding to a host of q_{Dy}. In the absence of strain (the black solid curve in Fig. 6), the envelop of CΦR distinctly deviates from a standard sinusoidal form due to the contributions stemming from higher harmonics [25,36]. Intriguingly, the deviation of CΦR is dramatically reduced with increasing q_{Dy}, indicating that the higher harmonics components can be pinched off by shifting Dirac points. Most importantly, the supercurrent is strongly suppressed by the shifting of Dirac points. In the regime of $q_{Dy} \geqslant k_0$, the Andreev excitations are completely forbidden, resulting in a on/off switch effect as exemplified in Fig. 7. This feature may be favorable for practical applications. Moreover, resorting to

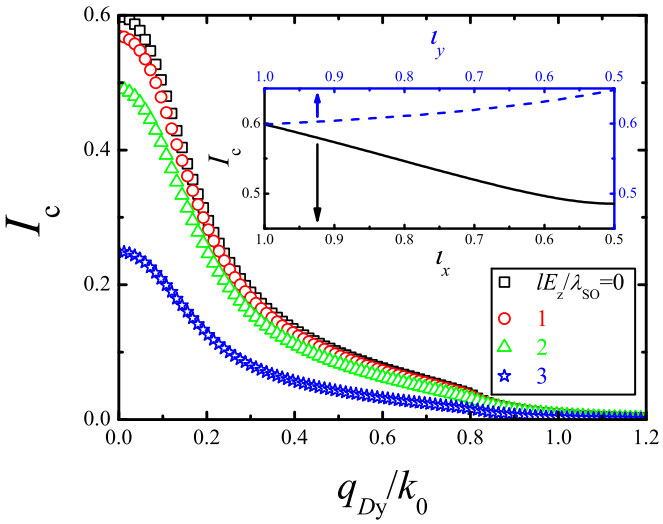

FIG. 7. Critical supercurrent as a function of the displacement of Dirac point. The inset shows the Fermi velocity-dependent critical supercurrent with $lE_z = 0$. As indicated by the arrows, the upper and lower horizonal axes in the inset refer to the blue dashed and black solid curves, respectively. The corresponding parameters are taken as the same values as those in Fig. 6.

the unique buckling structure of silicene, the strain dressed supercurrent can be modulated by an electric field.

The distortion of a Dirac cone can be parameterized by the Fermi velocity which can profoundly affect the current. According to Eq. (21), the x component of the current density operator can be derived as $J_x \propto \eta\iota_x v_F \sigma_z \otimes \tau_x$. As a consequence, the supercurrent decays with decreasing ι_x. Additionally, since the reduction of ι_y increases the number of Andreev channels, the supercurrent is enhanced by cutting down ι_y, as illustrated in the inset of Fig. 7.

IV. CONCLUSION

In conclusion, based on the DBdG equation, we investigate the influences of exchange splitting and electric field on the ABS and supercurrent in a silicene-based S/F/S junction. It is observed that a $0-\pi$ transition occurs with enhancing the exchange splitting, and the critical supercurrent at the transition point is nonvanishing. This characteristic may be favorable for fabricating dissipationless superconducting switches. Remarkably, the supercurrent can be effectively controlled by the electric field due to the buckling structure of silicene. In addition, it is found that the configuration of the supercurrent is dependent on the temperature. We also discuss the strain dressed supercurrent in a silicene-based S/strained/S junction. It is revealed that the CΦR strongly depends on the strain, and the supercurrent exhibits a switch effect with increasing the strength of strain. These findings would potentially give some insights into the correlated transport in silicene-based Josephson junctions.

ACKNOWLEDGMENTS

H.L. would like to thank L. Hao, H.-Y. Lu, Y. Y. Zhao, H.-X. He, and A. S. Cuamba for fruitful discussions. This work was supported by the Texas Center for Superconductivity at the University of Houston and the Robert A. Welch Foundation under Grant No. E-1146. The numerical calculations were performed at the Center of Advanced Computing and Data Systems at the University of Houston.

APPENDIX: BOUNDARY CONDITIONS AND ANDREEV BOUND STATES

In this appendix we perform necessary calculation details regarding the boundary conditions and ABSs. By matching the wave functions, the boundary conditions at $x = 0$ and $x = d$ are, respectively, given by

$$\begin{aligned}\sqrt{\hat{v}_S^x}\psi_S^L|_{x=0^-} &= \sqrt{\hat{v}_F^x}\psi_F|_{x=0^+},\\ \sqrt{\hat{v}_F^x}\psi_F|_{x=d^-} &= \sqrt{\hat{v}_S^x}\psi_S^R|_{x=d^+},\end{aligned} \tag{A1}$$

where $\hat{v}^x_{S(F)} = \partial\mathcal{H}_{S(F)}/\partial k_x$ is the x component of the velocity operator in the S (F) region. Equation (A1) automatically takes care of the current conservation in the x direction. These boundary conditions can also be rewritten as the forms given by Eqs. (9) and (10).

According to Eq. (13), the corresponding coefficients in Eq. (14) can be explicitly formulated as

$$\begin{aligned}\mathcal{A} = \cos\theta_+\cos\theta_- &- \frac{\sin\theta_+\sin\theta_-\cosh\gamma_+\cosh\gamma_-}{\cos^2\vartheta_S\cos\alpha_+\cos\alpha_-}\\ &+ \frac{\sin\vartheta_S\sin\theta_+\sin\theta_-(s_+s_-\sin\alpha_+\sin\alpha_-\sin\vartheta_S - s_-\sin\alpha_-\cosh\gamma_+ + s_+\sin\alpha_+\cosh\gamma_-)}{\cos^2\vartheta_S\cos\alpha_+\cos\alpha_-},\end{aligned} \tag{A2}$$

$$\begin{aligned}\mathcal{B} = &\frac{\cos\theta_-\sin\theta_+\cosh\gamma_+\cos\alpha_- + \cos\theta_+\sin\theta_-\cosh\gamma_-\cos\alpha_+}{\cos\vartheta_S\cos\alpha_+\cos\alpha_-}\\ &+ \frac{\tan\vartheta_S(s_-\sin\alpha_-\cos\alpha_+\cos\theta_+\sin\theta_- - s_+\sin\alpha_+\cos\alpha_-\cos\theta_-\sin\theta_+)}{\cos\alpha_+\cos\alpha_-},\end{aligned} \tag{A3}$$

$$\begin{aligned}\mathcal{C} = \cos\phi - \frac{\sin\theta_+\sin\theta_-}{\cos^2\vartheta_S}\Bigg(&-s_+s_-\tan\alpha_+\tan\alpha_-\\ &+ \frac{-\cos^2\vartheta_S\cosh(s_+\gamma_+ + s_-\gamma_-) + \cosh\gamma_+\cosh\gamma_- + \sin\vartheta_S(s_-\sin\alpha_-\cosh\gamma_+ - s_+\sin\alpha_+\cosh\gamma_-)}{\cos\alpha_+\cos\alpha_-}\Bigg).\end{aligned} \tag{A4}$$

[1] A. Kara, H. Enriquez, A. P. Seitsonen, L. C. Lew Yan Voon, S. Vizzini, B. Aufray, and H. Oughaddou, Surf. Sci. Rep. **67**, 1 (2012).

[2] S. Balendhran, S. Walia, H. Nili, S. Sriram, and M. Bhaskaran, Small **11**, 640 (2015).

[3] M. Houssa, A. Dimoulas, and A. Molle, J. Phys.: Condens. Matter. **27**, 253002 (2015).

[4] C. Grazianetti, E. Cinquanta, and A. Molle, 2D Mater. **3**, 012001 (2016).

[5] J. Zhao, H. Liu, Z. Yu, R. Quhe, S. Zhou, Y. Wang, C. C. Liu, H. Zhong, N. Han, J. Lu, Y. Yao, and K. Wu, Prog. Mater. Sci **83**, 24 (2016).

[6] B. Lalmi, H. Oughaddou, H. Enriquez, A. Kara, S. Vizzini, B. Ealet, and B. Aufray, Appl. Phys. Lett. **97**, 223109 (2010).

[7] P. Vogt, P. De Padova, C. Quaresima, J. Avila, E. Frantzeskakis, M. C. Asensio, A. Resta, B. Ealet, and G. Le Lay, Phys. Rev. Lett. **108**, 155501 (2012).

[8] N. Johnson, P. Vogt, A. Resta, P. D. Padova, I. Perez, D. Muir, E. Z. Kurmaev, G. L. Lay, and A. Moewes, Adv. Funct. Mater. **24**, 5253 (2014).

[9] A. Fleurence, R. Friedlein, T. Ozaki, H. Kawai, Y. Wang, and Y. Yamada-Takamura, Phys. Rev. Lett. **108**, 245501 (2012).

[10] L. Meng, Y. Wang, L. Zhang, S. Du, R. Wu, L. Li, Y. Zhang, G. Li, H. Zhou, W. A. Hofer, and H.-J. Gao, Nano Lett. **13**, 685 (2013).

[11] D. Chiappe, E. Scalise, E. Cinquanta, C. Grazianetti, B. Broek, M. Fanciulli, M. Houssa, and A. Molle, Adv. Mater. **26**, 2096 (2014).

[12] C.-C. Liu, H. Jiang, and Y. Yao, Phys. Rev. B **84**, 195430 (2011).

[13] C. L. Kane and E. J. Mele, Phys. Rev. Lett. **95**, 146802 (2005).

[14] C. L. Kane and E. J. Mele, Phys. Rev. Lett. **95**, 226801 (2005).

[15] C.-C. Liu, W. Feng, and Y. Yao, Phys. Rev. Lett. **107**, 076802 (2011).

[16] S. Cahangirov, M. Topsakal, E. Aktürk, H. Sahin, and S. Ciraci, Phys. Rev. Lett. **102**, 236804 (2009).

[17] N. D. Drummond, V. Zólyomi, and V. I. Fal'ko, Phys. Rev. B **85**, 075423 (2012).

[18] Z. Ni, Q. Liu, K. Tang, J. Zheng, J. Zhou, R. Qin, Z. Gao, D. Yu, and J. Lu, Nano Lett. **12**, 113 (2012).

[19] L. Tao, E. Cinquanta, D. Chiappe, C. Grazianetti, M. Fanciulli, M. Dubey, A. Molle, and D. Akinwande, Nat. Nanotech. **10**, 227 (2015).

[20] L.-D. Zhang, F. Yang, and Y. Yao, Sci. Rep. **5**, 8203 (2015).

[21] W. Wan, Y. Ge, F. Yang, and Y. Yao, Europhys. Lett. **104**, 36001 (2013).

[22] L. Chen, B. Feng, and K. Wu, Appl. Appl. Phys. Lett. **102**, 081602 (2013).

[23] J. Linder and T. Yokoyama, Phys. Rev. B **89**, 020504 (2014).

[24] K. K. Likharev, Rev. Mod. Phys. **51**, 101 (1979).

[25] A. A. Golubov, M. Yu. Kupriyanov, and E. ll'ichev, Rev. Mod. Phys. **76**, 411 (2004).

[26] A. F. Andreev, Sov. Phys. JETP **19**, 1228 (1964).

[27] B. Pannetier and H. Courtois, J. Low. Temp. Phys. **118**, 599 (2000).

[28] A. Furusaki and M. Tsukuda, Solid State Commun. **78**, 299 (1991).

[29] C. W. J. Beenakker and H. van Houten, Phys. Rev. Lett. **66**, 3056 (1991); C. W. J. Beenakker, *ibid.* **67**, 3836 (1991).

[30] V. V. Ryazanov, V. A. Oboznov, A. Yu. Rusanov, A. V. Veretennikov, A. A. Golubov, and J. Aarts, Phys. Rev. Lett. **86**, 2427 (2001).

[31] V. A. Oboznov, V. V. Bol'ginov, A. K. Feofanov, V. V. Ryazanov, and A. I. Buzdin, Phys. Rev. Lett. **96**, 197003 (2006).

[32] T. Champel, T. Löfwander, and M. Eschrig, Phys. Rev. Lett. **100**, 077003 (2008).

[33] G. Annunziata, H. Enoksen, J. Linder, M. Cuoco, C. Noce, and A. Sudbø, Phys. Rev. B **83**, 144520 (2011).

[34] Y. C. Tao, S. Y. Liu, N. Bu, J. Wang, and Y. S. Di, New J. Phys. **18**, 013010 (2015).

[35] R. Loria, C. Meneghini, K. Torokhtii, L. Tortora, N. Pompeo, C. Cirillo, C. Attanasio, and E. Silva, Phys. Rev. B **92**, 184106 (2015).

[36] J. Linder, T. Yokoyama, D. Huertas-Hernando, and A. Sudbø, Phys. Rev. Lett. **100**, 187004 (2008).

[37] A. G. Moghaddam and M. Zareyan, Phys. Rev. B **78**, 115413 (2008).

[38] M. Hu, X. Zhang, and D. Poulikakos, Phys. Rev. B **87**, 195417 (2013).

[39] B. Wang, J. Wu, X. Gu, H. Yin, Y. Wei, R. Yang, and M. Dresselhaus, Appl. Phys. Lett. **104**, 081902 (2014).

[40] X. Lin and J. Ni, J. Appl. Phys. **117**, 164305 (2015).

[41] J. A. Yan, S. P. Gao, R. Stein, and G. Coard, Phys. Rev. B **91**, 245403 (2015).

[42] C. W. J. Beenakker, Phys. Rev. Lett. **97**, 067007 (2006).

[43] H. B. Heersche, P. J. Herrero, J. B. Oostinga, L. M. K. Vandersypen, and A. F. Morpurgo, Nature (London) **446**, 56 (2007).

[44] X. Du, I. Skachko, and E. Y. Andrei, Phys. Rev. B **77**, 184507 (2008).

[45] T. Dirks, T. L. Hughes, S. Lal, B. Uchoa, Y.-F. Chen, C. Chialvo, P. M. Goldbart, and N. Mason, Nat. Phys. **7**, 386 (2011).

[46] K. Komatsu, C. Li, S. Autier-Laurent, H. Bouchiat, and S. Guéron, Phys. Rev. B **86**, 115412 (2012).

[47] D. K. Efetov, L. Wang, C. Handschin, K. B. Efetov, J. Shuang, R. Cava, T. Taniguchi, K. Watanabe, J. Hone, C. R. Dean, and P. Kim, Nat. Phys. **12**, 328 (2016).

[48] K. S. Novoselov, A. K. Geim, S. V. Morozov, D. Jiang, M. I. Katsnelson, I. V. Grigorieva, S. V. Dubonos, and A. A. Firsov, Nature (London) **438**, 197 (2005).

[49] F. Miao, W. Wijeratne, Y. Zhang, U. C. Coskun, W. Bao, and C. N. Lau, Science **317**, 1530 (2007).

[50] I. Žutić and O. T. Valls, Phys. Rev. B **61**, 1555 (2000).

[51] S. Wu and K. V. Samokhin, Phys. Rev. B **80**, 014516 (2009).

[52] M. Zareyan, H. Mohammadpour, and A. G. Moghaddam, Phys. Rev. B **78**, 193406 (2008).

[53] Y. Tanaka, T. Yokoyama, and N. Nagaosa, Phys. Rev. Lett. **103**, 107002 (2009).

[54] Z. Wang, C. Tang, R. Sachs, Y. Barlas, and J. Shi, Phys. Rev. Lett. **114**, 016603 (2015).

[55] G. E. Blonder, M. Tinkham, and T. M. Klapwijk, Phys. Rev. B **25**, 4515 (1982).

[56] M. Titov and C. W. J. Beenakker, Phys. Rev. B **74**, 041401 (2006).

[57] I. Hagymási, A. Kormányos, and J. Cserti, Phys. Rev. B **82**, 134516 (2010).

[58] J.-H. Choi, G.-H. Lee, S. Park, D. Jeong, J.-O. Lee, H.-S. Sim, Y.-J. Doh, and H.-J. Lee, Nat. Commun. **4**, 2525 (2013).

[59] B. Z. Rameshti, M. Zareyan, and A. G. Moghaddam, Phys. Rev. B **92**, 085403 (2015).
[60] J. Linder, Y. Tanaka, T. Yokoyama, A. Sudbø, and N. Nagaosa, Phys. Rev. B **81**, 184525 (2010).
[61] C. W. J. Beenakker, D. I. Pikulin, T. Hyart, H. Schomerus, and J. P. Dahlhaus, Phys. Rev. Lett. **110**, 017003 (2013).
[62] C. Kurter, A. D. K. Finck, Y. S. Hor, and D. J. Van Harlingen, Nat. Commun. **6**, 7130 (2015).
[63] P. A. Ioselevich, P. M. Ostrovsky, and M. V. Feigel'sman, Phys. Rev. B **93**, 125435 (2016).
[64] D. Kuzmanovski, J. Linder, and A. Black-Schaffer, arXiv:1605.03197.
[65] M. M. Fogler, F. Guinea, and M. I. Katsnelson, Phys. Rev. Lett. **101**, 226804 (2008).
[66] V. M. Pereira and A. H. Castro Neto, Phys. Rev. Lett. **103**, 046801 (2009).
[67] A. H. Castro Neto, F. Guinea, N. M. R. Peres, K. S. Novoselov, and A. K. Geim, Rev. Mod. Phys. **81**, 109 (2009).
[68] F. M. D. Pellegrino, G. G. N. Angilella, and R. Pucci, Phys. Rev. B **84**, 195404 (2011).
[69] C. Yesilyurt, S. G. Tan, G. Liang, and M. B. A. Jalil, Appl. Phys. Express **8**, 105201 (2015).